

Reactions of laser-ablated tellurium atoms with oxygen molecules: Matrix isolation infrared and DFT studies

K. Sundararajan *, K. Sankaran, V. Kavitha

Materials Chemistry Division, Indira Gandhi Centre for Atomic Research, Kalpakkam 603 102, India

Received 16 April 2007; received in revised form 19 June 2007; accepted 21 June 2007

Available online 30 June 2007

Abstract

Laser ablation of tellurium was carried out using the second harmonic Nd:YAG laser in the presence of oxygen molecules in argon/nitrogen matrices. The major species obtained in the Ar matrix were Te_2O_2 , TeO_2 , Te_2O_4 and the minor species were TeO , Te_2O and TeO_3 . In N_2 matrix, in addition to the above primary ablation products, reaction products TeN and Te_2N were also observed. The structure, energies and the vibrational frequencies of different tellurium oxide and nitride species were carried out using DFT calculations. The computed vibrational frequencies were corroborated with experimental frequencies.

© 2007 Elsevier B.V. All rights reserved.

Keywords: Laser ablation; Tellurium; Matrix isolation; Infrared

1. Introduction

Tellurium is one of the reactive fission products generated in the nuclear reactor. It is a highly volatile species and to study its behavior is of great concern under normal and in extreme conditions. Tellurium can form host of compounds with fuel and cladding materials [1]. Under off-normal conditions, tellurium might vaporize as tellurium dimer (Te_2) and as Te–O bearing species [2].

Muenow et al. [3] studied the vaporization, thermodynamics and structures of species in tellurium–oxygen system by Knudsen cell (K-cell) coupled with matrix isolation (MI) infrared technique. Fundamental frequencies obtained from the infrared absorptions for the different tellurium oxide species trapped at low temperature in argon and neon matrices were used for calculating the thermodynamic functions at various temperatures. From the mass spectrometric experiments, they concluded that the most abundant species formed were TeO and TeO_2 in the temperature range 782–903 K. Furthermore, they pre-

dicted TeO_2 to have a bent structure with a bond angle $110 \pm 3^\circ$ similar to that of SeO_2 . They have also assigned features due to tellurium monoxide dimers $(\text{TeO})_2$, tellurium dioxide dimers $(\text{TeO}_2)_2$ and trimers $(\text{TeO}_2)_3$ and predicted the structure of $(\text{TeO})_2$ dimer to be cyclic.

Spoliti et al. [4] used a similar technique as that of Muenow et al. and studied the spectrum of TeO_2 isolated in nitrogen matrix and assigned the features observed at 848.3, 831.7 and 294.0 cm^{-1} to the ν_3 , ν_1 and ν_2 modes of TeO_2 , respectively. From the vibrational data they calculated the gas phase vibrational frequencies of TeO_2 using the empirical relation reported by Hastie et al. [5].

Konings et al. [6] studied the vibrational spectrum of the TeO_2 vapor in a high temperature gas cell at 1250 K. They observed seven absorption bands which were assigned to three fundamental modes and four overtone/combination bands of gaseous TeO_2 . In another paper, Konings et al. [7] computed the structure of TeO_2 using coupled cluster CCSD(T) and MP2 methods. From the calculations at MP2 level, the vibrational frequencies of gaseous TeO_2 were reassigned. Several groups have carried out ab initio computations on tellurium dioxide and higher tellurium oxide clusters [8–12].

* Corresponding author.

E-mail address: sundar@igcar.gov.in (K. Sundararajan).

As can be seen, only K-cell coupled with MI infrared studies were carried out on TeO₂ in argon, nitrogen and neon matrices; and no laser ablation coupled with MI of Te + O₂ system was reported in the literature. We have therefore in the present work undertaken laser ablation of Te in the presence of O₂ in Ar/N₂ matrices and studied the species formed using infrared spectroscopic method. The objectives are: (1) to identify the reaction products of the laser-ablated species of Te + O₂ in Ar and N₂ matrices, (2) to compare the species produced in the laser ablation-MI of Te + O₂ with those of K-cell MI experiments on TeO₂, (3) to corroborate the experimental frequencies with the calculated frequencies for various tellurium oxide and nitride species and (4) to compare the various oxide and nitride species formed in tellurium with those of selenium.

2. Experimental

The technique of pulsed laser-ablation and matrix investigation used in these experiments was described elsewhere [13,14]. High-purity argon/nitrogen (Iolar, Grade I, M/s Bhoruka Gases Limited, India) and oxygen (Commercial Grade, M/s Inox Air Products, India) were used as matrix gases in these experiments.

The second harmonic (532 nm) of a pulsed Nd:YAG laser (Continuum, Model NY61-10), operated in the Q-switched mode, at a repetition rate of 10 Hz was used for ablation. The laser pulse had a temporal width of 10 ns. Typically, 20–40 mJ pulses were focused onto the sample, using a 100 mm focal length Suprasil lens. The laser beam was incident on the sample at a near-45° angle. The irradiance of such a focused beam was calculated to be 10⁸ W/cm², resulting in temperatures >2500 K at the focal point on the sample.

Pure tellurium powder (M/s Leico Industries Inc., USA, purity: 99.99%) dried under IR lamp and used for making the pellet. The pellet was sintered for 5 h under argon flow at 250 °C. The pellet was kept at a distance of 60 mm from the cold tip. The position of the laser beam on the sample was varied manually to expose a fresh surface to the laser beam continuously. This arrangement ensured efficient ablation during the entire course of the experiment.

The laser-ablated species from the sample were deposited along with Ar/N₂ at a rate of ~3 mmol/h onto a 12 K KBr window for 1–2 h. Infrared spectrum of the deposited species was recorded using a BOMEM MB100 FTIR, operating at a resolution of 1 cm⁻¹. Photolysis was carried out using a 150 W broad band Xe UV source (M/s Spectral Energy Inc.) and annealing cycles at 25 K were also carried out and an infrared spectrum was again recorded.

All our experiments were performed using ¹⁴N₂ and ¹⁶O₂. Due to non-availability of ¹⁵N₂ and ¹⁸O₂ we could not perform the isotopic experiments.

3. Computations

The geometries and vibrational frequencies of various tellurium oxide and nitride species were calculated using

DFT/B3LYP method. The LanL2DZ basis sets built in the Gaussian-98 program [15] were employed for the tellurium atoms and aug-cc-PVDZ basis sets were employed for the oxygen and nitrogen atoms. Calculations were also performed using LanL2DZdp ECP polarization functions for tellurium atoms taken from EMSL basis set library [16]. Tables 1 and 2 give the structural parameters, vibrational frequencies and the zero-point corrected (ZPE) energies for the various tellurium oxide and nitride species using LanL2DZ basis sets for tellurium whereas Tables 3 and 4 give the frequencies using LanL2DZdp basis sets. Figs. 1 and 2 show the structures of different tellurium oxide and nitride species obtained by DFT method.

4. Results and discussion

Initially, the infrared spectra of laser-ablated products of Te + O₂ reaction in argon and nitrogen matrices will be presented and later the vibrational assignments for the observed bands with DFT calculations using LanL2DZ basis sets for the tellurium atoms and the reaction mechanisms for the formation of various tellurium oxide species will be discussed.

4.1. Te + O₂/Ar system

Fig. 3a shows the infrared spectra of laser-ablated Te(s) deposited using 10% O₂ in argon matrix and the product absorption bands are listed in Table 5. The major peaks are observed at 1074.2, 1039.0, 841.4 and 617.7 cm⁻¹. In addition, we also observed a number of peaks with moderate to weak intensities at 886.2, 881.4, 865.0, 858.7, 823.5, 782.5, 591.6 and 538.6 cm⁻¹. The features due to ozone (O₃) in argon matrix were observed at 1039.0 and 702.5 (not shown) cm⁻¹ [17]. The spectral feature observed at 782.5 cm⁻¹ is due to TeO and the features observed at 841.4 and 823.5 cm⁻¹ are assigned to the ν_3 and ν_1 vibrations of TeO₂ in Ar matrix. These assignments were based on the earlier K-cell coupled with matrix isolation infrared experiments, where the vapor phase species over TeO₂(s) at a maximum temperature of 973 K were trapped in argon and neon matrices [3,4]. We also observed the combination bands $2\nu_1 - \nu_2$ and $\nu_1 + \nu_2$ of TeO₂ in argon matrix at 1328.3 and 1111.4 cm⁻¹ that agreed well with the earlier reported values [7]. Fig. 3b shows the infrared spectrum recorded after the matrix was annealed at 25 K for 15 min. As can be seen from the spectrum that there is no substantial change in intensities of the peaks because of annealing. Fig. 3c shows the spectrum after the matrix was photolysed using a broadband UV source for 15 min. On photolysis, features at 1074.2 and 782.5 cm⁻¹ vanished completely whereas features at 886.2, 881.4, 841.4, 617.7, 591.6 and 538.6 cm⁻¹ gained in intensity. On further annealing the matrix at 25 K for 15 min (Fig. 3d), all the major peaks gained very less intensity when compared to the photolysed spectra.

Table 1
Frequency (cm^{-1}), intensity (km/mol), and structure calculations for diatomic, triatomic and tetraatomic tellurium–oxygen compounds using B3LYP method

Molecule	Frequencies (intensity)	Bond lengths (\AA) ^d	Bond angle ($^\circ$)	Energy (hartrees) ^e
TeO (a)	787.5(14)	1.825	–	–83.19820
OTeO ^a (b)	284.3(27), 850.0(10), 863.7(84)	1.782	111.6	–158.44797
Cyclic-O ₂ Te ^a (c)	492.5(3), 609.7(14), 906.4(21)	2.003	68.5	–158.36191
TeOO ^a (d)	313.7(0), 547.3(17), 1203.1(384)	2.005, 1.275	127.5	–158.34826
Cyclic-TeTeO ^b (e)	199.2(1), 482.0(1), 575.2 (34)	2.022, 2.766	46.9	–91.286699
TeTeO ^b (f)	126.7(5), 198.1(11), 787.1(97)	2.758, 1.810	130.5	–91.282526
TeOTe ^b (g)	141.6(1), 428.0(14), 662.8(71)	1.954	131.5	–91.270955
TeO ₃ ^c (h)	174.3(38), 260.6(30), 260.7(30), 810.4(0), 864.3(57), 864.5(57),	1.775	120.0	–233.59075
<i>cis</i> -OOTeO ^c (i)	118.4(3), 262.9(5), 336.9(0), 525.0(20), 849.6(68), 1139.1(333)	1.295, 2.000, 1.783	120.2, 104.9, 0.0 ^f	–233.56122
<i>trans</i> -OOTeO ^c (j)	144.2(14), 178.4(3), 294.4(5), 535.6(7), 844.8(87), 1096.4(361)	1.308, 1.993, 1.786	118.2, 103.5, 180.0 ^f	–233.55779
OOOTe ^c (k)	113.2(0), 165.0(0), 228.9(3), 488.1(8), 739.8(25), 1435.0(788),	1.220, 1.698, 1.888	112.7, 116.7	–233.50130
Exocycle Te ₂ O ₂ ^g (l)	129.4(1), 179.9(11), 238.4(16), 473.3(9), 585.8(36), 856.5(98)	2.070, 1.945, 1.779, 2.843	46.7, 111.3	–166.50413
Cyclic(TeO) ₂ ^g (m)	187.7 (0), 258.5(0), 298.6(0), 363.5(128), 499.2(68), 701.6(0)	1.999	106.5, 73.5, 0.0 ^f	–166.49535
TeOTeO ^g (n)	94.7(1), 100.7(0), 184.7(5), 445.6(19), 624.5(59), 838.8(132)	1.998, 1.914, 1.788	129.5, 103.4, 179.9 ^f	–166.48866
TeTeOO ^g (o)	75.0(3), 138.7(0), 207.2(4), 257.2(2), 495.6(9), 1159.3(645)	2.662, 2.061, 1.287	101.4, 119.2, 180.0 ^f	–166.41778
(TeO) ₂ (p)	75.6(12), 157.8(21), 191.6(0), 228.4(0), 284.3(0), 326.7(50), 467.6(0), 534.9(90), 617.2(437), 632.1(0), 879.1(136), 880.3(0)	1.973, 1.769	100.7, 79.2, 103.9, 101.8 ^f , –101.8 ^f	–316.97586

LanL2DZ basis set was used for tellurium and aug-cc-PVDZ for oxygen atom.

^a Relative energy of isomers 0, +54, +63 kcal/mol going down the column.

^b Relative energy of isomers 0, +3, +10 kcal/mol going down the column.

^c Relative energy of isomers 0, +19, +21, +56 kcal/mol going down the column.

^d Bond lengths given for molecule, left to right, respectively.

^e ZPE corrected energy.

^f Dihedral angle.

^g Relative energy of isomers 0, +6, +10, +54 kcal/mol going down the column.

4.2. Te + O₂/N₂ system

Fig. 4a shows the infrared spectra of laser-ablated Te(s) using 10% O₂ in nitrogen matrix and the product absorption bands are listed in Table 6. Features due to common species of nitrogen oxides such as NO, N₂O, NO₂ were observed at 1874.6, 2235.0, 1616.2 and the nitrogen radicals N₃[·] and N₃[−] at 1657.6 and 2003.4 cm^{-1} , respectively, which agree well with the reported values [18,19]. In N₂ matrix, the strongest bands were observed at 1074.2, 1042.9 and 848.1 cm^{-1} (Fig. 4a). The features due to ozone (O₃) in nitrogen matrix were observed at 1042.9 and 704.5 cm^{-1} (not shown) [17]. We also observed features with moderate intensities at 1575.2, 973.5, 790.3, 784.0 and 778.7 cm^{-1} and with very weak features at 538.6, 588.2, 623.4, 619.6 and 881.4 cm^{-1} . The features observed at 848.1 and 833.2 cm^{-1} were due to ν_3 and ν_1 vibrations of TeO₂ in N₂ matrix [4]. On annealing the matrix at 25 K (Fig. 4b) the changes in the intensities of all the features were moderate. On photolysis (Fig. 4c), the intensity of features at 881.4, 623.4/619.6 and 538.6 cm^{-1} increased

substantially but the features at 778.7, 1074.2 and 1575.2 cm^{-1} vanished completely. On further annealing (Fig. 4d) the matrix at 25 K for 15 min all the major features gained very less intensities when compared to the photolysed spectra.

4.3. Vibrational assignments for each tellurium oxide and nitride species

4.3.1. TeO

The feature observed at 782.5 cm^{-1} (Ar) and 778.7 cm^{-1} (N₂) bands are assigned to the tellurium monoxide, which is in good agreement with the previous reported values [3]. The DFT calculations using aug-cc-PVDZ basis sets predicted a value of 787.5 cm^{-1} , which corroborates well with the observed value. The calculated bond length between Te and O atoms is 1.825 \AA and agrees well with the experimental value of 1.828 \AA [20]. Ab initio computation by Noguera et al. [12] using B3LYP/3-21G** basis set on TeO predicted the fundamental to occur at 795 cm^{-1} . Tellurium monoxide may be produced by the reaction (1), which is

Table 2

Frequency (cm^{-1}), intensity (km/mol), and structure calculations for diatomic and triatomic tellurium–nitrogen compounds using B3LYP method

Molecule	Frequencies (intensity)	Bond lengths (\AA) ^d	Bond angle ($^\circ$)	Energy (hartrees) ^e
TeN (a)	757.5(14)	1.856,	–	–62.70963
TeNTe ^a (b)	152.1(3), 383.5(10), 860.9(268)	1.911	143.7	–70.801000
TeTeN ^a (c)	110.5(3), 161.0(13), 830.5(58)	3.019, 1.825	110.6	–70.744593
NNTe ^b (d)	356.8(2), 357.5(3), 389.6(10), 2195.4(432)	1.126, 2.000	180.0	–117.54872
N ₂ Te ^b (e)	193.2(3), 288.6(5), 2105.4(176)	1.136, 2.432	76.4	–117.51248
NTeN ^b (f)	66.7(14), 816.4(0), 881.4(16)	1.813	170.7	–117.30861
TeNO ^c (g)	349.4(1), 463.1(35), 1694.8(775)	2.008, 1.181	138.9	–137.95553
NTeO ^c (h)	205.8(18), 582.4(8), 789.7(30)	1.804, 1.939	108.1	–137.89474

LanL2DZ basis set was used for tellurium and aug-cc-PVDZ for oxygen and nitrogen atoms.

^a Relative energy of isomers 0, +35, +166 kcal/mol going down the column.^b Relative energy of isomers 0, +23, +150 kcal/mol going down the column.^c Relative energy of isomers 0, +38 kcal/mol going down the column.^d Bond lengths given for molecule, left to right, respectively.^e ZPE corrected energy.

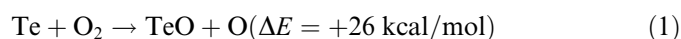
Table 3

Frequency (cm^{-1}), intensity (km/mol), calculations for diatomic, triatomic and tetraatomic tellurium–oxygen compounds using B3LYP method

Molecule	Frequencies (intensity)
TeO (a)	802.9(21)
OTeO (b)	277.5(28), 848.4(10), 867.5(93)
Cyclic-O ₂ Te (c)	499.6(6), 616.5(14), 895.9(19)
TeOO (d)	312.3(0), 543.6(16), 1191.3(371)
CyclicTeTeO (e)	212.9(1), 466.4(6), 585.5(36)
TeTeO (f)	146.6(7), 225.3(12), 781.3(106)
TeOTe (g)	136.8(1), 413.5(14), 673.7(62)
TeO ₃ (h)	192.7(36), 264.0(30), 264.4(30), 810.3(0), 871.4(58), 871.8 (58)
<i>cis</i> -OOTeO (i)	118.4(3), 265.5(5), 337.0(0), 516.7(21), 857.2(70), 1126.2(321)
<i>trans</i> -OOTeO (j)	137.1(12), 175.0(3), 286.8(5), 533.3(7), 852.4(92), 1085.7(349)
OOOTe (k)	110.4(0), 155.5(1), 225.4(2), 497.3(6), 734.9(24), 1453.4(841)
Exocycle-Te ₂ O ₂ (l)	138.9(2), 194.8(14), 227.7(15), 456.5(12), 587.6(40), 857.8(103)
Cyclic(TeO) ₂ (m)	185.2(0), 258.8(0), 296.6(29), 356.9(136), 500.9(66), 690.9(0)
TeOTeO (n)	84.8(1), 99.4(0), 178.3(5), 420.4(15), 636.8(58), 846.2(141)
TeTeOO (o)	76.2(4), 137.2(0), 227.2(5), 262.3(3), 496.6(7), 1122.3(628)
(TeO ₂) ₂ (p)	80.0(12), 153.1(20), 186.4(0), 221.4(0), 278.7(0), 320.2(48), 457.4(0), 533.2(86), 610.7(436), 615.1(0), 877.6(145), 879.7(0)

LanL2DZdp basis set was used for tellurium and aug-cc-PVDZ for oxygen atom.

endothermic by +26.9 kcal/mol [21–23] and this excess energy can be obtained from the laser-ablated plumes.



4.3.2. TeO₂

Computations predicted three possible isomers for the TeO₂; OTeO, cyclic-TeOO and TeOO. Fig. 1b–d shows the structure of these isomers and Table 1 gives the geometrical parameters, vibrational frequencies and the ZPE corrected energies for these isomers. For the lowest energy

Table 4

Frequency (cm^{-1}), intensity (km/mol), and energy calculations for diatomic and triatomic tellurium–nitrogen compounds using B3LYP method

Molecule	Frequencies (intensity)
TeN (a)	767.9(11)
TeNTe (b)	150.2(4), 377.6(11), 887.5(264)
TeTeN (c)	126.8(6), 213.6(1), 567.2(16)
NNTe (d)	351.2(1), 351.6(1), 391.5(10), 2192.0(438)
N ₂ Te (e)	194.6(3), 295.8(5), 2094.0(188)
NTeN (f)	66.7(14), 816.4(0), 881.4(16)
TeNO (g)	351.7(1), 461.1(34), 1689.5(787)
NTeO (h)	200.6(19), 602.6(8), 806.7(38)

LanL2DZdp basis set was used for tellurium and aug-cc-PVDZ for oxygen and nitrogen atoms.

isomer OTeO, DFT calculations predicted the bond length between Te and O to be 1.782 \AA and the bond angle $\angle\text{OTeO}$ to be 111.6 $^\circ$ clearly showing the molecule to have a bent structure. Earlier calculations on TeO₂ by Konings et al. [7] and Noguera et al. [12] also predicted similar results.

The 841.4, 823.5 cm^{-1} (Ar) and 848.1, 833.2 cm^{-1} (N₂) features were assigned to the ν_3 and ν_1 modes of TeO₂, respectively. These assignments agree well with the earlier K-cell coupled with matrix isolation experiments [3,4]. The calculated frequencies for $\nu_3 = 863.7 \text{ cm}^{-1}$ and $\nu_1 = 850.0 \text{ cm}^{-1}$ modes are higher than those observed in argon matrix by 2.6%, 3.2% and in nitrogen matrix by 1.8%, 2.0%, respectively. The agreement is excellent considering the approximations involved in the DFT calculation. The observed increase in TeO₂ features in both the matrices could probably be due to the insertion of tellurium atom into the oxygen molecule under UV irradiation. TeO₂ can be formed by the following reaction (2)



The other two possible isomers for the TeO₂ are cyclic-OTeO and TeOO which are less stable by 54 and 63 kcal/mol. Experimentally, we have not discerned any feature corresponding to these isomers.

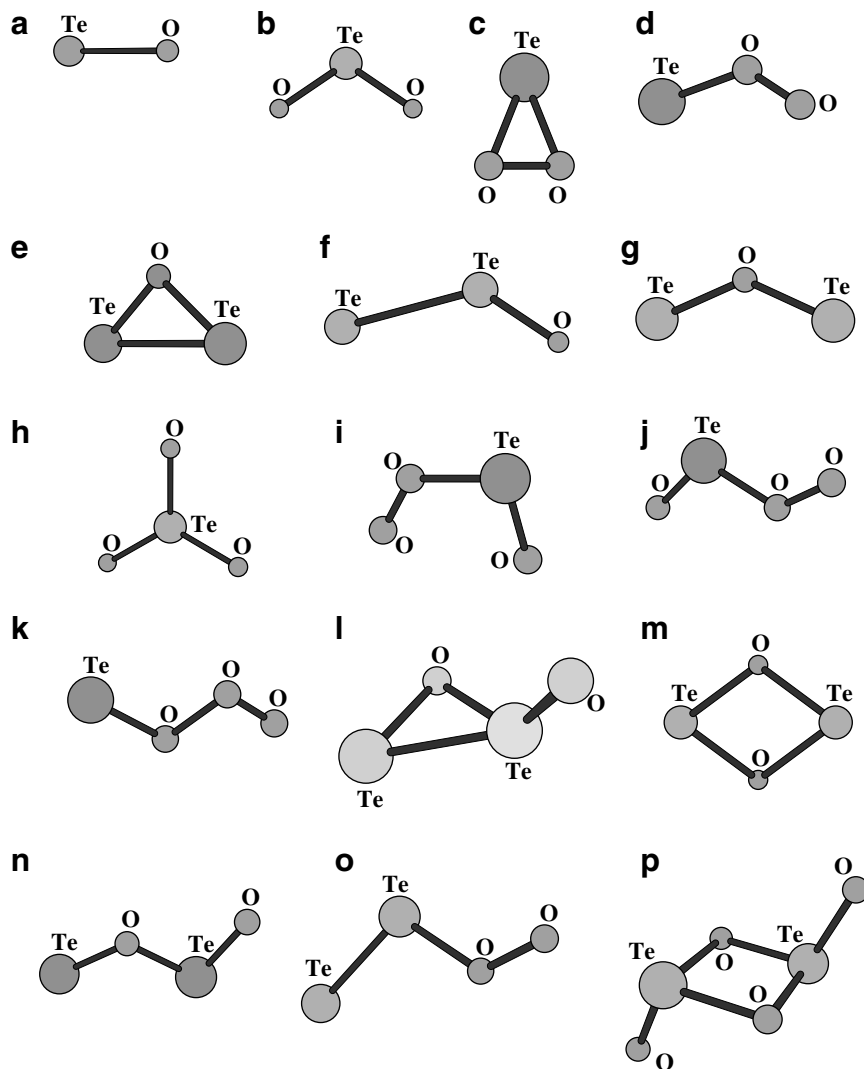


Fig. 1. Structures of the different tellurium oxide species calculated at B3LYP/aug-cc-PVDZ method.

4.3.3. TeO_3

DFT calculations predicted four possible isomers for TeO_3 ; planar- TeO_3 , *cis*- $OTeOO$, *trans*- $OTeOO$ and $OOOTe$. Fig. 1h–k shows the structure of the isomers and Table 1 gives the structural parameters, frequencies and ZPE corrected energies for all the isomers. DFT computations for the TeO_3 (D_{3h}) showed the bond angle between O–Te–O to be 120.0° and the bond distance between Te and O to be 1.775 \AA , which is a global minima on the potential energy surface. The other three isomers are higher in energy and less stable by 19–60 kcal/mol when compared to the planar- TeO_3 isomer. The calculated frequencies for the TeO_3 isomer occur as a doubly degenerate Te–O stretching mode at 864.3 and 864.5 cm^{-1} . Experimentally, we observed a doublet feature at 858.7 and 865.0 cm^{-1} in Ar matrix and both these features increased in intensity on photolysis and annealing cycle experiments as well, clearly indicating that they belong to the same species. As can be seen from the Table 6 that there is a very good agreement between the calculated and experimental frequencies. Hence, we assign the features observed at 858.7 and

865.0 cm^{-1} in Ar matrix to TeO_3 isomer. In the N_2 matrix, we could not observe the features due to TeO_3 isomer, probably the isomer being unstable. A similar result was obtained for the UO_3 species when uranium oxide was laser ablated in nitrogen matrices [13]. Experimentally, we have not discerned any feature corresponding to the other TeO_3 isomers.

4.3.4. Te_2O_2

Calculations predicted the most stable Te_2O_2 isomer to be an exocycle- Te_2O_2 similar to that of exocycle- Se_2O_2 [24] with a C_1 symmetry; it has a three-membered TeTeO ring and contains an exocyclic-Te=O unit (Fig. 1l). The next higher energy isomer has a four-membered cyclic structure, which is less stable by 6 kcal/mol. Muenow et al. [3] assigned features observed near 520.0 and 650.0 cm^{-1} to the cyclic $(TeO)_2$ and predicted TeOTe bond angle to be 100° . Their assignments were based on the results obtained for analogous cyclic- $(SnO)_2$ [25]. DFT calculations also predicted two other possible isomers, TeO–TeO and TeTeOO which are less stable by 10 and

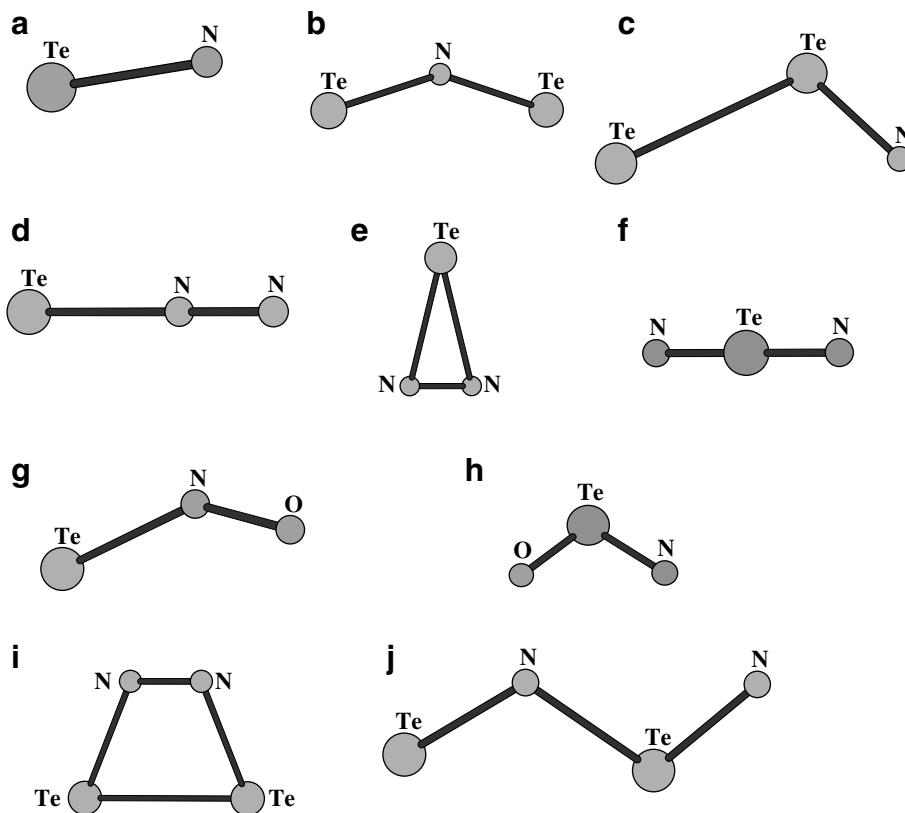


Fig. 2. Structures of the different tellurium nitride species calculated at B3LYP/aug-cc-PVDZ method.

50 kcal/mol, respectively. Fig. 11–o shows the structures of different Te_2O_2 isomers.

In our laser-ablation experiment of Te(s) in 10% O_2/Ar or N_2 we observed a very strong feature at 1074.2 (Ar) and 1073.7 (N_2) cm^{-1} in the as-deposited spectra. On photolysis this feature vanished completely in both the matrices, clearly showing that the feature is unstable on UV irradiation. Barbson et al. [24] studied the species formed when selenium was discharged/heated in the presence of O_2 in argon matrix. They observed a new feature at 1404.5 cm^{-1} and have assigned it to $(\text{Se}_2)(\text{O}_2)$. On vacuum-UV photolysis, the intensity of this feature decreased and a new feature was observed at 1061 cm^{-1} which they have assigned to SeOO species. Even though we might be tempted to assign the observed features at 1074.2(Ar) and 1073.7(N_2) to TeOO isomer similar to SeOO species, we have assigned them to the TeTeOO based on the following reasoning: it is well known fact that $\text{Te}_2(\text{g})$ is the major species in the vapor phase over Te(s) [23]. In our laser-ablation experiments too there is a very high probability of formation of Te_2 , which might further react with O_2 to form TeTeOO according to the reaction (3).



As per the DFT calculations, the stretching fundamental frequencies for the TeTeOO isomer (1159.3 cm^{-1}) is much closer ($\sim 7.0\%$) to the experimental frequency than for TeOO (1203.1 cm^{-1} ; $\sim 11\%$) isomer. Hence, we assign the observed features to TeTeOO.

4.3.5. Te_2O

DFT calculations have predicted the most stable isomer of Te_2O to be a cyclic-TeTeO. The cyclic- Te_2O isomer has a stretching fundamental at 575.2 cm^{-1} . We observed a very weak feature at 591.6 cm^{-1} (Ar) and 588.2 cm^{-1} (N_2). This feature gained in intensity on annealing cycle and photolysis. The calculated value agrees well within 2.7% (Ar) and 2.2% (N_2) when compared with the experimental frequencies. Hence, we assign the feature observed to the cyclic- Te_2O isomer.

DFT calculations also predicted a bent TeTeO molecule with a strong Te–O fundamental at 787.1 cm^{-1} , which is very close to the TeO frequency at 787.5 cm^{-1} and the “open” or “ozone-like” TeOTe isomer with a feature at 662.8 cm^{-1} . These two species are less stable by 2–10 kcal/mol. We did not discern any vibrational features due to these species. Fig. 1e–g shows the structures and Table 1 gives the ZPE corrected energies of all the three isomers.

4.3.6. Te_2O_4

DFT calculations have predicted a cyclic structure for the Te_2O_4 species. Fig. 1p shows the structure of the Te_2O_4 , which contains four Te–O bonds in the ring and two Te–O bonds in the axial positions, and Table 1 gives the structural parameters, vibrational frequencies and the ZPE corrected energies. We observed features at 881.4, 617.7, 538.6 in

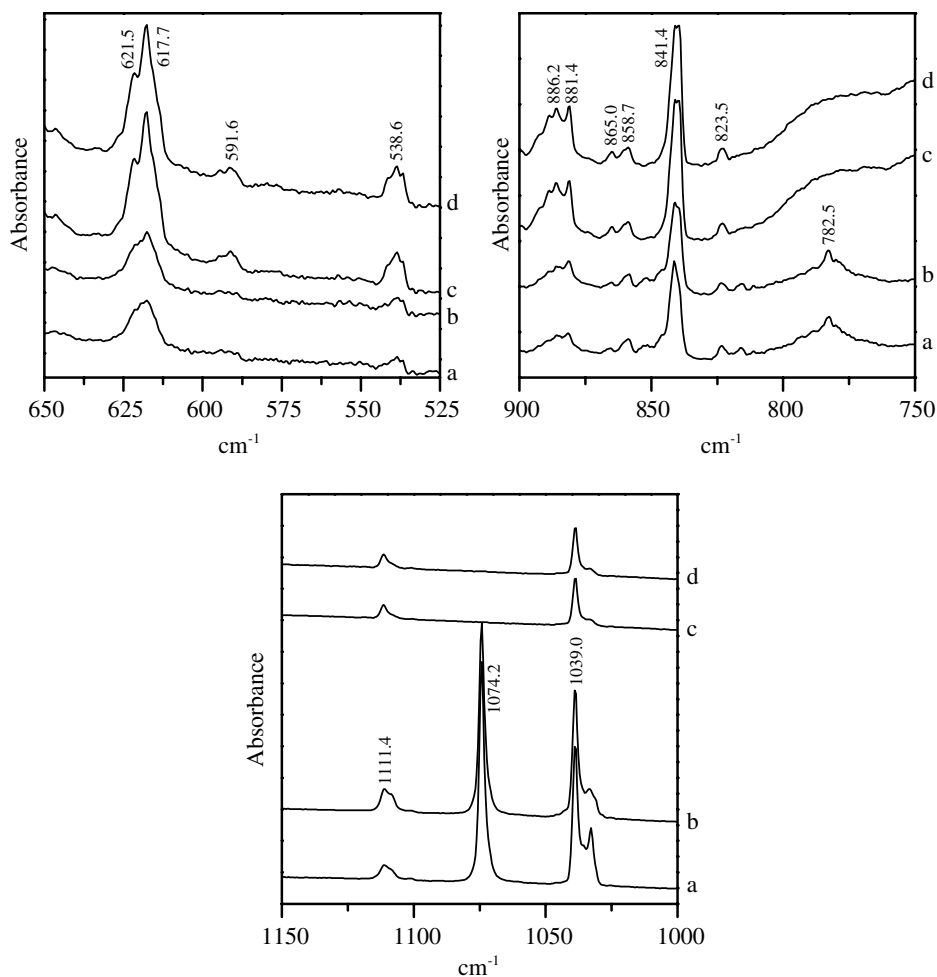


Fig. 3. Matrix isolation infrared spectra of laser-ablated Te in the region 650–525, 900–750 and 1150–1000 cm^{-1} using O_2/Ar mixed matrix. Concentration of O_2 in the O_2/Ar was 10%. (a) As deposited, (b) 25 K annealed, (c) photolysed and (d) 25 K annealed.

Table 5
Infrared absorptions (cm^{-1}) observed for Te + O_2 in argon matrix

Frequencies (cm^{-1})	Assignments
1328.3	TeO_2 , $2\nu_1 - \nu_2$
1111.4	TeO_2 , $\nu_1 + \nu_2$
1074.2	Te_2O_2
1039.0	O_3
886.2, 881.4	$(\text{TeO}_2)_2$
865.0, 858.7	TeO_3
841.4	TeO_2 , ν_3
823.1	TeO_2 , ν_1
782.5	TeO
662.5	TeOTe
617.7	$(\text{TeO}_2)_2$
538.6	$(\text{TeO}_2)_2$
591.6	Cyclic- TeTeO

argon and at 881.4, 619.6, 538.6 in N_2 matrix. Fig. 5 (block A and block B) shows the behavior of these features during annealing cycle and photolysis in Ar and N_2 matrices. As can be seen, in both the matrices all the three features behaved similarly during annealing cycle as well as on photolysis ascertaining that these features belong to the same

species. The calculated frequencies for Te_2O_4 has the strongest features at 879.1, 617.2 and 534.9 cm^{-1} which are lower by 0.3%, 0.1% and 0.6%, respectively, when compared with the experimental frequencies.

The increase in Te_2O_4 features on photolysis can be explained based on the fact that the TeO_2 formation in the matrix is increased on photolysis due to (1) Possible insertion of Te atom into the oxygen molecule as per reaction (4) and (2) Breaking of Te–Te bonds and possible rearrangement to form TeO_2 and Te in the matrix as per reaction (5). The excess TeO_2 formed in the above reactions in the matrix might undergo dimerization to form Te_2O_4 according to the reaction. (6)



4.3.7. TeN

The calculations predict TeN fundamental to occur at 757.5 cm^{-1} . We observed split features in N_2 matrix at

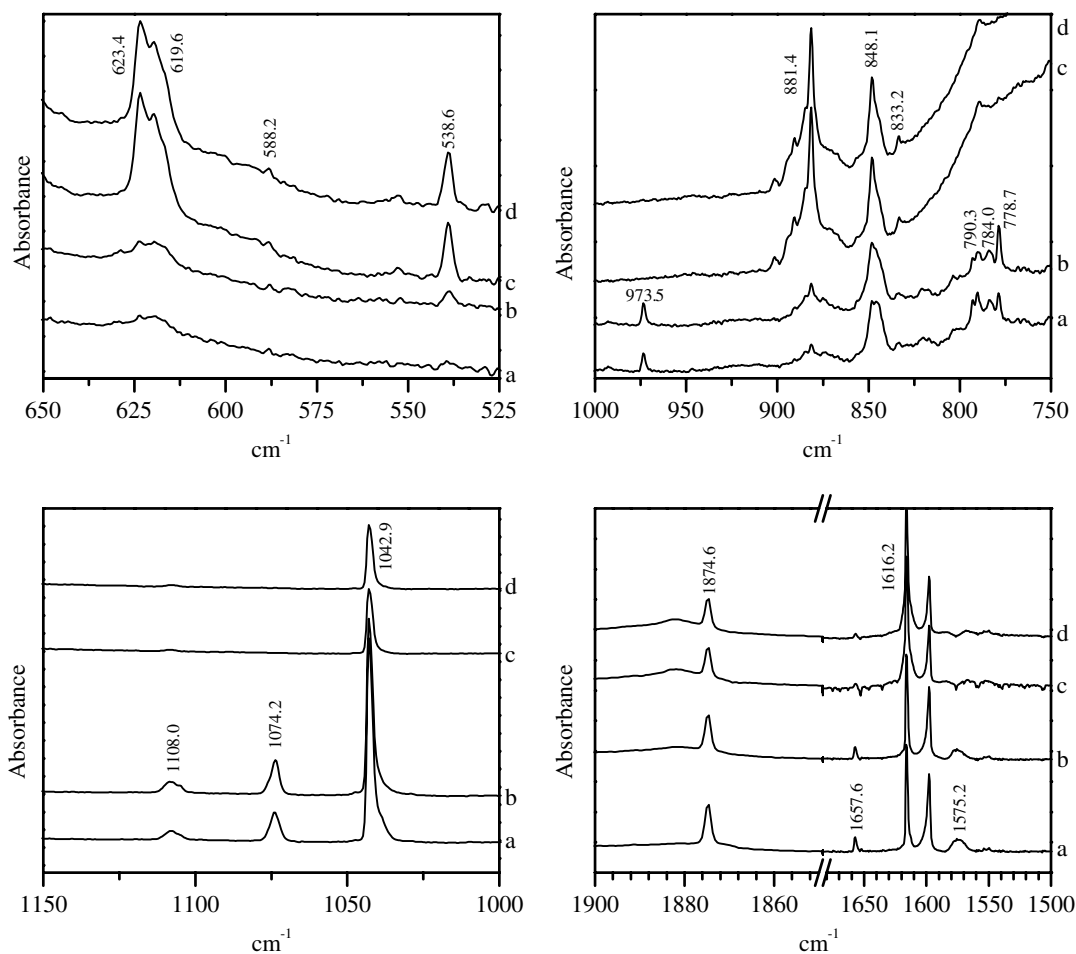


Fig. 4. Matrix isolation infrared spectra of laser-ablated Te in the region 650–525, 1000–750, 1150–1000 and 1900–1500 cm^{-1} using O_2/N_2 mixed matrix. Concentration of O_2 in the O_2/N_2 was 10%. (a) As deposited, (b) 25 K annealed, (c) photolysed and (d) 25 K annealed.

Table 6

Infrared absorptions (cm^{-1}) observed for Te+ O_2 in nitrogen matrix

Frequencies (cm^{-1})	Assignments
1874.6	NO
2235.0	N_2O
1616.2	NO_2
1657.2	N_3^+
2003.4	N_3^-
1575.2	TeNO
1108.0	$\text{TeO}_2, \nu_1 + \nu_2$
1074.2	Te_2O_2
1042.9	O_3
973.5	TeNTe
881.4	$(\text{TeO}_2)_2$
848.1	TeO_2, ν_3
833.2	TeO_2, ν_1
778.7	TeO
790.3	TeN site 1
784.0	TeN site 2
662.0	TeOTe
623.4/619.6	$(\text{TeO}_2)_2$
538.6	$(\text{TeO}_2)_2$
588.2	Cyclic-TeTeO

790.3 and 783.5 cm^{-1} . The calculated frequencies are lower than the experimental values by 4.3% and 3.3%, respectively. Similar site split feature has also been reported for

SN [26] and SeN molecules [27,28]. Fig. 4 shows the infrared spectrum over the above regions when tellurium was laser ablated in the presence of 10% O_2/N_2 . The occurrence of spectral feature at 1657.6 and 2003.4 cm^{-1} are clear signatures of the presence of N_3^+ and N_3^- and (not shown) in our laser ablation of Te with 10% O_2/N_2 experiment provides a strong support for the formation of TeN as was observed in the case of UN [14]. Fig. 2a shows the structure and Table 2 gives the ZPE corrected energy for the TeN species.

4.3.8. NTe_2

DFT calculations predicted two possible isomers for NTe_2 . Of these, the bent TeNTe structure is the global minima. The angle between the Te–N–Te was calculated to be 143.7°, which is very similar to the bent SeNSe molecule [27]. Fig. 2b–c show the structure of the isomers, Table 2 gives the vibrational frequencies, the geometries and the ZPE corrected energies. The calculated Te–N stretching frequency occurs at 860.9 cm^{-1} which is 12% lower compared to the experimentally observed feature at 973.5 cm^{-1} . The other isomer with a bent TeTeN structure is less stable by 35 kcal/mol and the calculated vibrational

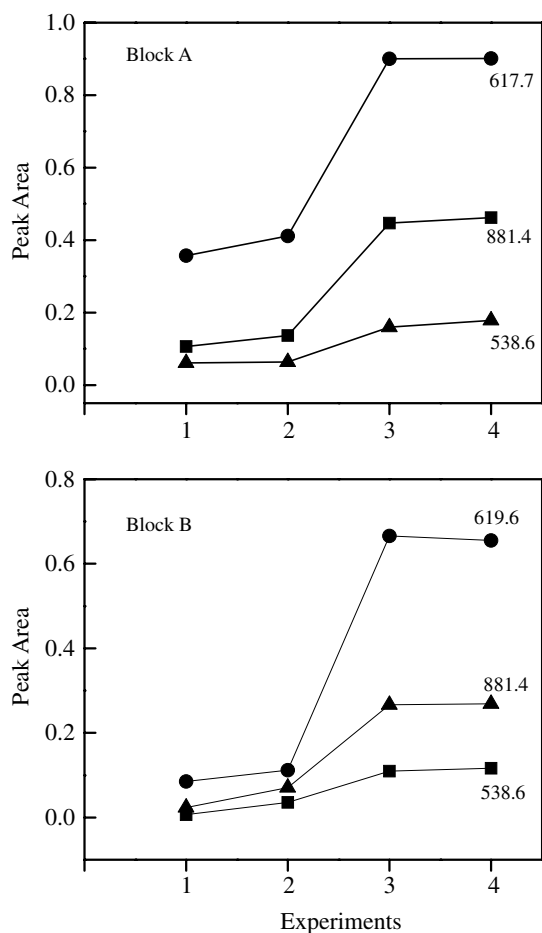


Fig. 5. Areas of the different peaks in Ar matrix (block A) and N₂ matrix (block B) for various experimental conditions: (1) as deposited, (2) annealed at 25 K, (3) photolysed and (4) annealed at 25 K after photolysis. Concentration of O₂ in the both the matrices was 10%.

frequency occur at 830.5 cm⁻¹. Hence, we assign the feature observed at 973.5 cm⁻¹ to the bent TeNTe molecule.

4.3.9. N₂Te

According to DFT calculations there are three possible isomers for N₂Te. Fig. 2e–f shows the structure of these isomers. Of these, the linear TeNN and cyclic-TeNN isomers have an infrared active N₂ perturbation mode at 2195.4 and 2105.4 cm⁻¹. The other isomer, linear NTeN is less stable by 150 kcal/mol and has a Te–N fundamental at 881.4 cm⁻¹. Experimentally, we could not discern any features corresponding to these isomers.

4.3.10. TeNO

Of the two possible isomers predicted by DFT calculations, the one with Te attached to NO is the global minima. Fig. 2g–h shows the structures of these isomers. The bond distance between the Te and NO is 2.0 Å and the bond angle is 138.9°. These data indicate that the molecule is bent and is similar to the structure of bent SeNO molecule [27]. Calculations predicted a very strong fundamental band for the NO stretching mode to occur at

1694.8 cm⁻¹. Experimentally, we observed a feature at 1575.7 cm⁻¹ in the as-deposited spectrum, which is lower than the calculated value by about 7.5%. On photolysis the intensity of this feature decreased considerably. We assign the observed feature at 1575.7 cm⁻¹ to the N–O stretching mode of the bent TeNO molecule analogous to the SNO and SeNO species [26,27].

4.3.11. Te_xN_y species

DFT calculations were also performed for the higher tellurium nitrides as well. Two of these structures are given in Fig. 2i–j and the corresponding parameters in Table 2. Experimentally, we could not discern any features corresponding to the higher Te–N clusters.

5. Comparison of different oxide and nitride species formed between tellurium and selenium

Barbison et al. [24] studied the species formed when selenium was discharged/heated with oxygen in argon matrix. They observed SeO, SeO₂, SeO₃, (Se₂)(O₂), SeSeO, SeOO, exocycle-Se₂O₂ and *cis*-OSeOO, with (Se₂)(O₂) being the major species. In our experiments, we observed species due to TeO, TeO₂, TeO₃, Te₂O₂, Te₂O₄ and TeTeO with Te₂O₂ as the major species. As can be seen, the Te + O analogs of SeOO, exocycle-Se₂O₂ and *cis*-OSeOO were not observed. However, we could observe higher tellurium oxide cluster (Te₂O₄). In Se₂O isomers, bent SeSeO isomer is the most stable one whereas in the case of Te₂O the cyclic-TeTeO isomer is the most stable species.

Selenium with N₂ forms [27,28] a variety of products such as SeN, Se₂N, NSe₂⁺, SeSeN, *cis*-SeSeNSe, *trans*-SeSeSeN and SeNO whereas in Te with 10% O₂/N₂ experiments we could identify species only due to TeN, Te₂N and TeNO. We found no evidences for higher tellurium nitride clusters.

6. Conclusion

This study reports for the first time the matrix isolation infrared spectra of the laser-ablated tellurium oxide species in argon and nitrogen matrices. The primary reaction products obtained in the Ar and N₂ matrices are Te₂O₂, TeO, TeO₂, Te₂O and Te₂O₄. In N₂ matrix, in addition to the primary laser-ablated products, reaction products TeN, TeNTe and TeNO were also observed. While the identification of TeO and TeO₂ species agreed with the Knudsen cell-MI experiments [3], we also observed some exotic reaction products such as Te₂O₂, cyclic-TeTeO and Te₂O₄ and these features were corroborated with the help of computations. When compared to the reactivity of selenium and tellurium towards nitrogen, tellurium is less reactive whereas selenium forms host of higher selenium nitride species.

Acknowledgements

V.K. gratefully acknowledges the grant of a research fellowship from the Council of Scientific and Industrial

Research (CSIR), India. We thank Dr. T.S. Lakshminarasimhan, IGCAR, Kalpakkam for useful discussion in preparing the manuscript.

References

- [1] H. Kleykamp, *J. Nucl. Mater.* 131 (1985) 221.
- [2] B.R. Bowsher, S. Dickinson, A.L. Nichols, R.A. Gomme, J.S. Ogden, Anon.-American Chemical Society, Division of Nuclear Chemistry and Technology, Washington, DC (USA), in: *Proceedings of the Symposium on Chemical Phenomenon Associated with Radioactivity Releases During Severe Nuclear Plant Accidents*, Anaheim, CA, American Chemical Society, September 8–12, 1986.
- [3] D.W. Muenow, J.W. Hastie, R. Hauge, R. Bautista, J.L. Margrave, *Trans. Faraday Soc.* 65 (1969) 3210.
- [4] M. Spoliti, S.N. Cesaro, E. Coffari, *J. Chem. Thermodyn.* 4 (1972) 507.
- [5] J.W. Hastie, R.H. Hauge, J.L. Margrave, *Inorg. Chem.* 1 (1970) 57.
- [6] R.J.M. Konings, E.H.P. Cordfunke, A.S. Booij, *Chem. Phys. Lett.* 167 (1990) 499.
- [7] R.J.M. Konings, A.S. Booij, A. Kovács, *Chem. Phys. Lett.* 292 (1998) 447.
- [8] A. Strömberg, O. Gropen, U. Wahlgren, *J. Chem. Phys.* 80 (1984) 1593.
- [9] H. Basch, D. Cohen, M. Albeck, *Chem. Phys. Lett.* 144 (1988) 450.
- [10] J. Jánky, R.H. Bartram, A.R. Rossi, G. Corradi, *Chem. Phys. Lett.* 124 (1986) 26.
- [11] R. Custodio, W.M. Davis, John D. Goddard, *J. Mol. Struct. (Theochem)* 315 (1994) 163.
- [12] O. Noguera, M. Smirnov, A.P. Mirgorodsky, T. Merle-Méjean, P. Thomas, J.-C. Champarnaud-Mesjard, *Phys. Rev. B* 68 (2003) 094203.
- [13] K. Sankaran, K. Sundararajan, K.S. Viswanathan, *Bull. Mater. Sci.* 22 (1999) 785.
- [14] K. Sankaran, K. Sundararajan, K.S. Viswanathan, *J. Phys. Chem. A* 105 (2001) 3995.
- [15] M.J. Frisch, G.W. Trucks, H.B. Schlegel, G.E. Scuseria, M.A. Robb, J.R. Cheeseman, V.G. Zakrzewski, J.A. Montgomery Jr, R.E. Stratmann, J.C. Burant, S. Dapprich, J.M. Millam, A.D. Daniels, K.N. Kudin, M.C. Strain, O. Farkas, J. Tomasi, V. Barone, M. Cossi, R. Cammi, B. Mennucci, C. Pomelli, C. Adamo, S. Clifford, J. Ochterski, G.A. Petersson, P.Y. Ayala, Q. Cui, K. Morokuma, D.K. Malick, A.D. Rabuck, K. Raghavachari, J.B. Foresman, J. Cioslowski, J.V. Ortiz, A.G. Baboul, B.B. Stefanov, G. Liu, A. Liashenko, P. Piskorz, I. Komaromi, R. Gomperts, R.L. Martin, D.J. Fox, T. Keith, M.A. Al-Laham, C.Y. Peng, A. Nanayakkara, M. Challacombe, P.M. W. Gill, B. Johnson, W. Chen, M.W. Wong, J.L. Andres, C. Gonzalez, M. Head-Gordon, E.S. Replogle, J.A. Pople, *Gaussian 98*, Revision A.9, Gaussian Inc., Pittsburgh PA, 1998.
- [16] Basis sets were obtained from the Extensible Computational Chemistry Environment Basis Set Database, Version 02/02/06, as developed and distributed by the Molecular Science Computing Facility, Environmental and Molecular Sciences Laboratory which is part of the Pacific Northwest Laboratory, P.O. Box 999, Richland, Washington 99352, USA, and funded by the US Department of Energy. The Pacific Northwest Laboratory is a multi-program laboratory operated by Battelle Memorial Institute for the US Department of Energy under contract DE-AC06-76RLO 1830.
- [17] L. Schriver-Mazzuoli, A. Schriver, C. Lugez, A. Perrin, C. Camy-Peyret, J.-M. Flaud, *J. Mol. Spectrosc.* 176 (1996) 85.
- [18] W.G. Fateley, Henry A. Bent, B. Crawford Jr., *J. Chem. Phys.* 31 (1959) 204.
- [19] R. Tian, J.C. Facelli, J. Michl, *J. Phys. Chem.* 92 (1988) 4073.
- [20] G.G. Chandler, H.J. Hurst, R.F. Barrow, *Proc. Phys. Soc. Lond.* 86 (1998) 447.
- [21] T.S. Lakshmi Narasimhan, M. Sai Baba, R. Viswanathan, *Thermochim. Acta* 427 (2005) 137.
- [22] O. Kubaschewski, C.B. Alcock, *Metallurgical Thermochemistry*, fifth ed., Pergamon press, Oxford, 1979.
- [23] F. Grønvold, J. Drowart, E.F. Westrum Jr., *The chemical thermodynamics of actinide elements and compounds, Part 4*, in: *The Actinide Chalcogenides (Excluding Oxides)*, IAEA, Vienna, 1984.
- [24] G. Dana Brabson, L. Andrews, C.J. Marsden, *J. Phys. Chem.* 100 (1996) 16487.
- [25] J.S. Anderson, J.S. Ogden, M.J. Ricks, *Chem. Commun.* 24 (1968) 1585.
- [26] P. Hassanzadeh, L. Andrews, *J. Am. Chem. Soc.* 114 (1992) 83.
- [27] L. Andrews, P. Hassanzadeh, D.V. Lanzisera, G.D. Brabson, *J. Phys. Chem.* 100 (1996) 16667.
- [28] L. Andrews, P. Hassanzadeh, *J. Chem. Soc. Chem. Commun.* (1994) 1523.